J Nanostruct 14(3): 765-779, Summer 2024

RESEARCH PAPER

# Preparation and Investigation of Structural and Optical Properties of PVA/$Y_2O_3$/$SrCO_3$ Nanocomposites and Apply as the Antibacterial

*Ali Salim Jwad* *, *Ali Razzaq Abdulridha*

*Department of Physics, College of Education for Pure Sciences, University of Babylon, Babylon, Iraq*

**ARTICLE INFO**

***Article History:***
*Received 06 April 2024*
*Accepted 23 June 2024*
*Published 01 July 2024*

***Keywords:***
*FESEM*
*FTIR*
*Optical Characteristic*
*PVA*
*$SrCO_3$ NPs*
*$Y_2O_3$ NPs*

**ABSTRACT**

This paper outlines the process of creating polyvinyl alcohol (PVA) composites by adding different amounts (0, 1, 2, 3, and 4) of $Y_2O_3$ and $SrCO_3$ nanoparticles (NPs) by the solution casting method. The OM pictures demonstrated the emergence of interconnected pathways inside the polymeric matrix as electrically charged particles, which intensified with greater concentrations of nanoparticles. The structural features of the nanocomposite were analyzed using Fourier transformation spectroscopy (FTIR) to obtain information on molecular vibration. FTIR analysis revealed that the polymer matrix exhibited interactions with the added $Y_2O_3$ and $SrCO_3$ nanoparticles. The FTIR analysis has shown the existence of physical interactions between $Y_2O_3$ and $SrCO_3$ nanoparticles and the PVA polymer matrix. The nanocomposite surface was analyzed using Field Emission Scanning Electron Microscopy (FESEM). It was discovered that the $Y_2O_3$ and $SrCO_3$ nanoparticles were evenly and uniformly dispersed throughout the PVA polymer matrix. An increase in the ratio of $Y_2O_3$ and $SrCO_3$ nanoparticles in the PVA led to an increase in absorbance, absorption coefficient, refractive index, extinction coefficient, real and energy band gap. However, the transmittance and indirect energy gap decreased. The absorbance coefficient is below $10^4$ $cm^{-1}$, indicating an occurrence of indirect electron transition. Finally, the PVA/$Y_2O_3$/$SrCO_3$ nanocomposites were tested for the antibacterial against both gram positive Staphylococcus aureus (S. aureus) and gram-negative Escherichia coli (E. coli). The result obtained that the inhibition zone diameter increased with increasing $Y_2O_3$ and $SrCO_3$ NPs. The PVA/$Y_2O_3$/$SrCO_3$ nanocomposite exhibited antibacterial activity.

**How to cite this article**
*Jwad A., Abdulridha A. Preparation and Investigation of Structural and Optical Properties of PVA/$Y_2O_3$/$SrCO_3$ Nanocomposites and Apply as the Antibacterial . J Nanostruct, 2024; 14(3):765-779. DOI: 10.22052/JNS.2024.03.007*

## INTRODUCTION

Polymer nanocomposites are polymers that have been improved by adding fillers with various shapes (such as platelets, fibers, spheroids, etc.) that are less than 100 nm in at least one dimension [1]. Nanocomposites, formed by the amalgamation of diverse materials, architectures, and compositions, exhibit a wide range of properties that are well-suited for numerous applications. Consequently, there has been significant attention towards multifunctional materials in the nanocomposite industry [2].

Polyvinyl alcohol (PVA) is a polymer that has attracted significant interest from researchers due

* *Corresponding Author Email: pure.ali.razaq@uobabylon.edu.iq*

to its unique physical and chemical characteristics [3]. Polyvinyl alcohol (PVA) is a versatile polymer that finds use in several sectors. The primary variables that contribute to this phenomenon are their exceptional optical characteristics, low weight, and excellent mechanical attributes. Polyvinyl alcohol (PVA) finds widespread use in diverse applications, including adhesives, medication delivery systems, coatings, and fuel cells. Due of the robust hydrogen bonds formed by hydroxyl groups, both internally and externally, PVA has a high melting point that closely approximates its breakdown temperature. Because of this characteristic, the melting process of PVA poses challenges, which is why it is more advantageous to process it from solutions in water [4]. Due to its compatibility with the human body, it can also serve as a medicinal material [5]. In addition, PVA has the ability to specifically adsorb metallic ions such as copper, palladium, and mercury. Polyvinyl alcohol (PVA) is a polymer with the chemical formula $(C_2H_4O)x$. The substance has a density ranging from 1.19 to 1.31 g/cm$^3$ and a melting point of 230℃. This thermoplastic polymer undergoes rapid degradation when exposed to temperatures above 200℃. The structure of this substance is pliable and is determined by the presence of C–O–C links. Moreover, it has the ability to dissolve in organic solvents, a tendency to interact with water, a crystalline structure, and the potential to offer self-lubrication [6].

Yttrium oxide ($Y_2O_3$) is one of the most important advanced ceramic materials. In addition, ($Y_2O_3$) is preferred as host material due to its excellent chemical durability, high thermal stability, high refractory property, corrosion resistivity, low phonon energy, high refractive index [7]. $Y_2O_3$ (III) oxide (also Known as yttria, diyttrium trioxide, yttrium sesquioxide, and $Y_2O_3$ is an air stable, water insoluble oxide that has various applications in material science and inorganic chemistry [8].

Strontium carbonate ($SrCO_3$) is regarded as a highly promising compound because of its diverse range of properties, such as a high dielectric constant, a high dispersion frequency constant, and a low temperature coefficient [9]. Strontium carbonate is essential in the current electrical and glass industries as a key component [10]. In addition, the distinct crystal structure of strontium carbonate has been extensively studied as a representative system for bio-crystallization [11]. Several systematic methods, including self-assembly monolayers [12], thermos evaporated stearic membrane [13], and polyanionic additives [14], have been developed to improve the formation of crystalline $SrCO_3$ from a water-based solution [15].

In this paper, preparation of the PVA/$Y_2O_3$/$SrCO_3$ nanocomposite and investigate the structural and optical properties and apply as antibacterial.

## MATERIALS AND METHODS

### *Materials*

Pure PVA (Alpha Chemika, India) with average molecular weight 18000 g/mol are applied as granular form. Yttrium oxide nanoparticles ($Y_2O_3$NPs) (Sigma Aldrich) with purity 99.8%, is a white powder that is insoluble in water and particle size 30 nm. Strontium carbonate nanoparticles ($SrCO_3$ NPs) (Sigma Aldrich) with purity 99.899%, is a white powder that is insoluble in water and particle size 50 nm.

### *Purification of nanocomposites*

1g of PVA was dissolved in 50 mL of distilled water firstly for 30 minutes at RT, then continue for another 20 minutes under 75-80°C using magnetic stirrer until to PVA solvent. The resulting solution was cast onto clean glasses Petri dish and kept it under air at RT for 240h for drying process till the solvent gets completely evaporated. PVA with $Y_2O_3$ and $SrCO_3$ NPs were fellow the same

Table 1 Summarized the purification of pure PVA and nanocomposite films.

| PVA (g) | $Y_2O_3$ (g) | $SrCO_3$ (g) |
|---|---|---|
| 1 | 0 | 0 |
| 0.98 | 0.01 | 0.01 |
| 0.96 | 0.02 | 0.02 |
| 0.94 | 0.03 | 0.03 |
| 0.92 | 0.04 | 0.04 |

procedure to prepare nanocomposite films. The method summarized in Table 1. The thickness of the produced films was about 0.12 mm.

*Descriptions*

To show the chemical make-up of the samples that were prepared, FTIR (Bruker business, type vertex -70 spectrometer, German origin) was used at room temperature, covering the range of 4000-500 $cm^{-1}$. To determine the surface morphology of the films, researchers used a (FESEM, INSPECT S50, firm, Japan origin, type FEI Customer ownership). A Shimadzu UV-1650 PC spectrophotometer, manufactured by Phillips, a Japanese corporation, was used to examine the development of nanocomposite at wavelengths ranging from 200 to 1100 nm.

## RESULT AND DISCUSSION

The optical microscope reveals changes in the surface morphology of (PVA/ $Y_2O_3$/ $SrCO_3$) nanocomposites. Fig. 1 depicts the

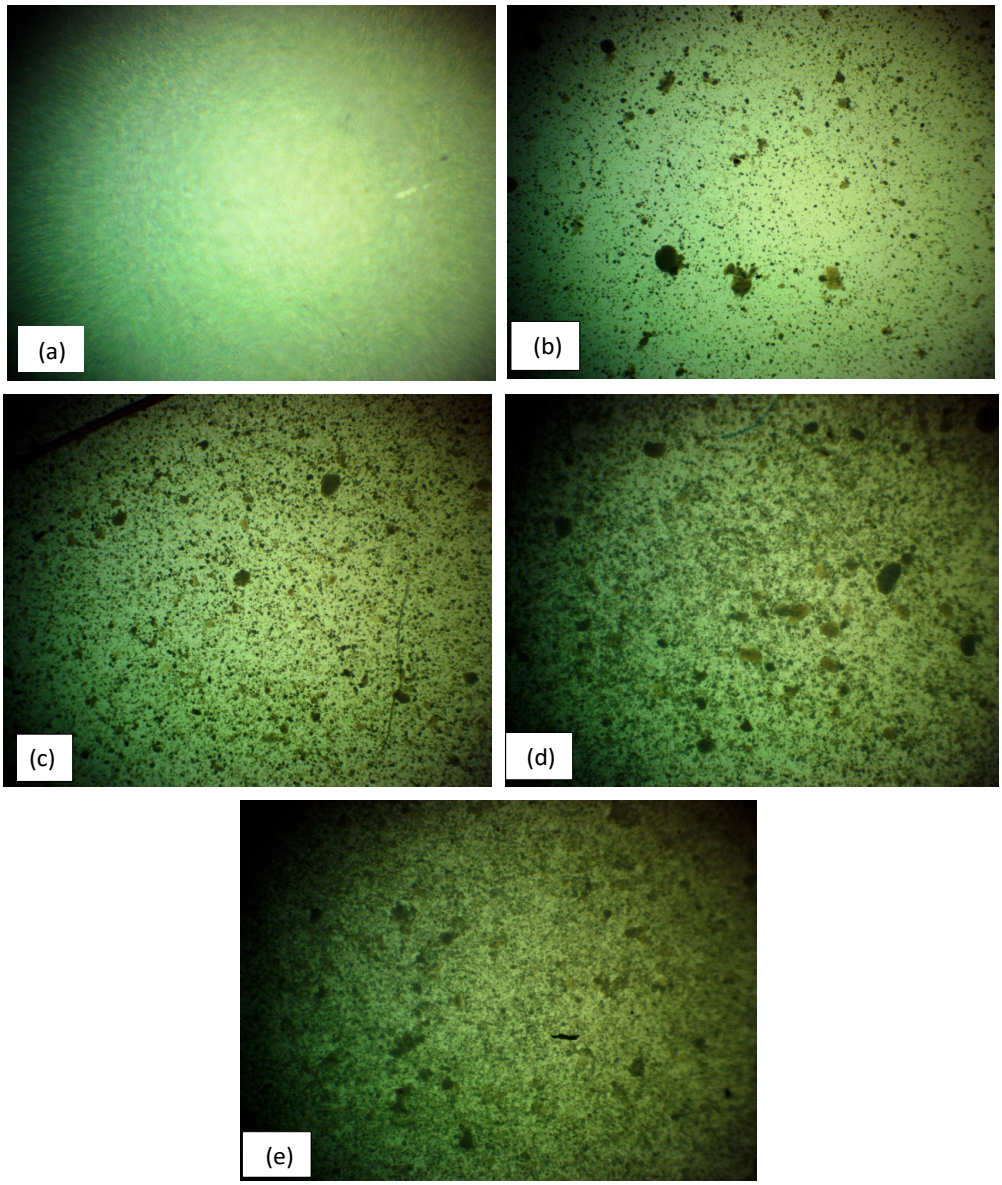


Fig. 1. Optical microscope for the (a) pure PVA, (b) 1 wt.% $Y_2O_3$ and $SrCO_3$ NPs, (c) 2 wt.% $Y_2O_3$ and $SrCO_3$ NPs, (d) 3 wt.% $Y_2O_3$ and $SrCO_3$ NPs, (e) 4wt.% $Y_2O_3$ and $SrCO_3$ NPs

nanocomposites (PVA/ $Y_2O_3$/ $SrCO_3$) captured using an optical microscope (OM) at a 10x magnification. Image (a) illustrates a uniform phase without any separation of phases. Furthermore, it displays a more elegant form and a sleek texture, suggesting the effective polymer ratio of PVA. Based on the photos (b-e), it is apparent that the ($Y_2O_3$/ $SrCO_3$) nanoparticles exhibit a uniform distribution on the PVA polymer film surface. This phenomenon gets more noticeable as the weight proportion of ($Y_2O_3$/ $SrCO_3$) increases. The surface pictures of nanoparticles exhibit a distinct and consistent

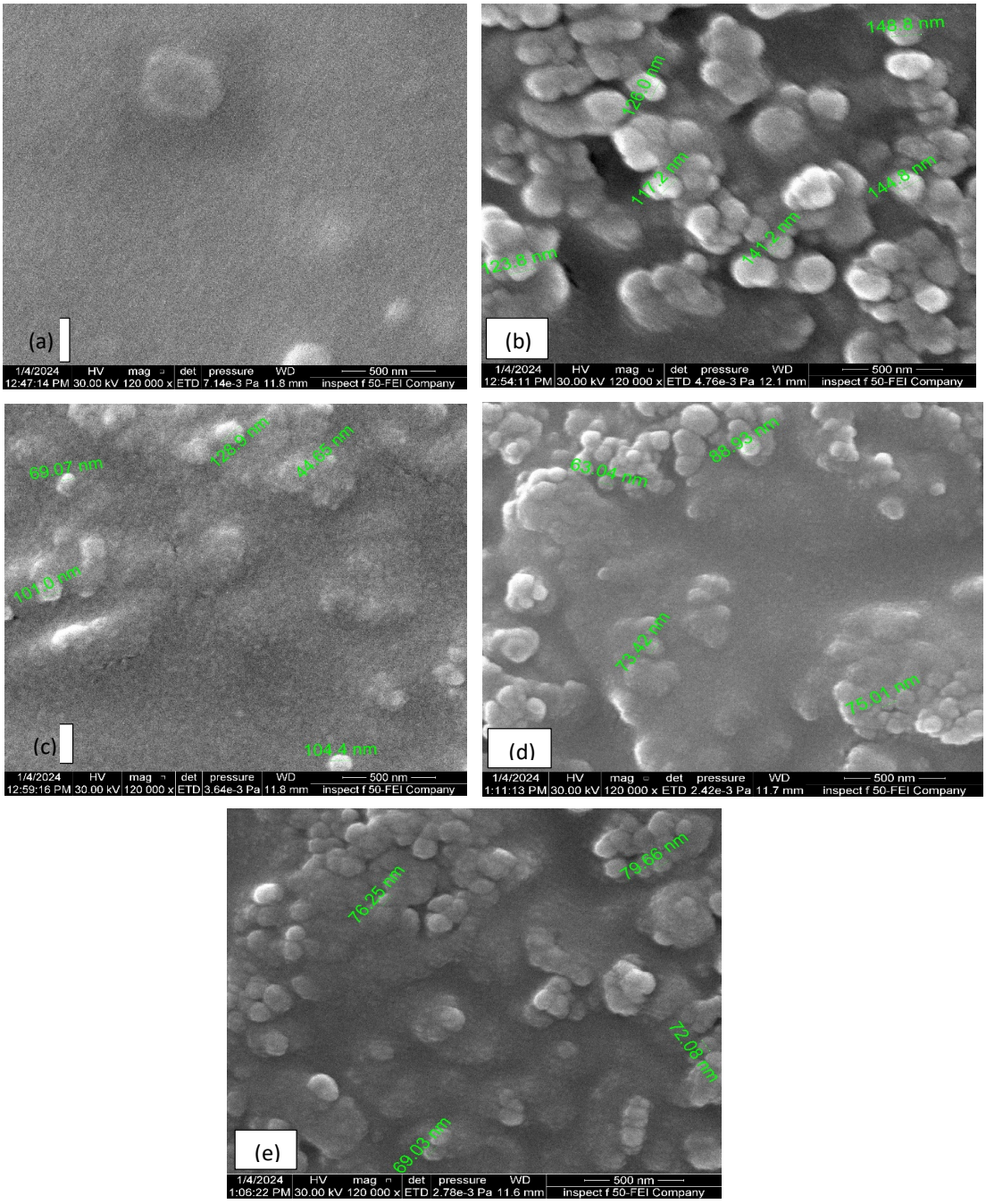


Fig. 2. FESEM images for the (a) pure PVA, (b) 1 wt.% $Y_2O_3$ and $SrCO_3$ NPs, (c) 2 wt.% $Y_2O_3$ and $SrCO_3$ NPs, (d) 3 wt.% $Y_2O_3$ and $SrCO_3$ NPs, (e) 4wt.% $Y_2O_3$ and $SrCO_3$ NPs

distribution of grain density, suggesting a surface morphology that is more uniform and homogeneous. At lesser concentrations, the nanoparticles exhibit a disorganized arrangement, forming aggregates that are randomly scattered on the surface of the film. Nevertheless, when the concentration of additive nanoparticles rises, they establish an intricate network of interconnecting pathways within the polymeric blend. This technology provided a suitable method for creating nanocomposite films [16,17].

FESEM is used for the purpose of examining the distribution of nanoparticles within the polymer, and then verifying the effect of those particles of $Y_2O_3$/$SrCO_3$ on those nanocomposites. Fig. 2 shows FESEM images of films made from (PVA/$Y_2O_3$/$SrCO_3$) nanocomposites with varying amounts of $Y_2O_3$ and $SrCO_3$ NPs with a magnification 20 KX and scale 500 nm. Image (a) indicate that the surface polymer is smooth and homogenous which indicate that successful method, while in images (b, c, d and e), the $Y_2O_3$ and $SrCO_3$ distributed through the polymer matrix. Also, it can be obtained that the

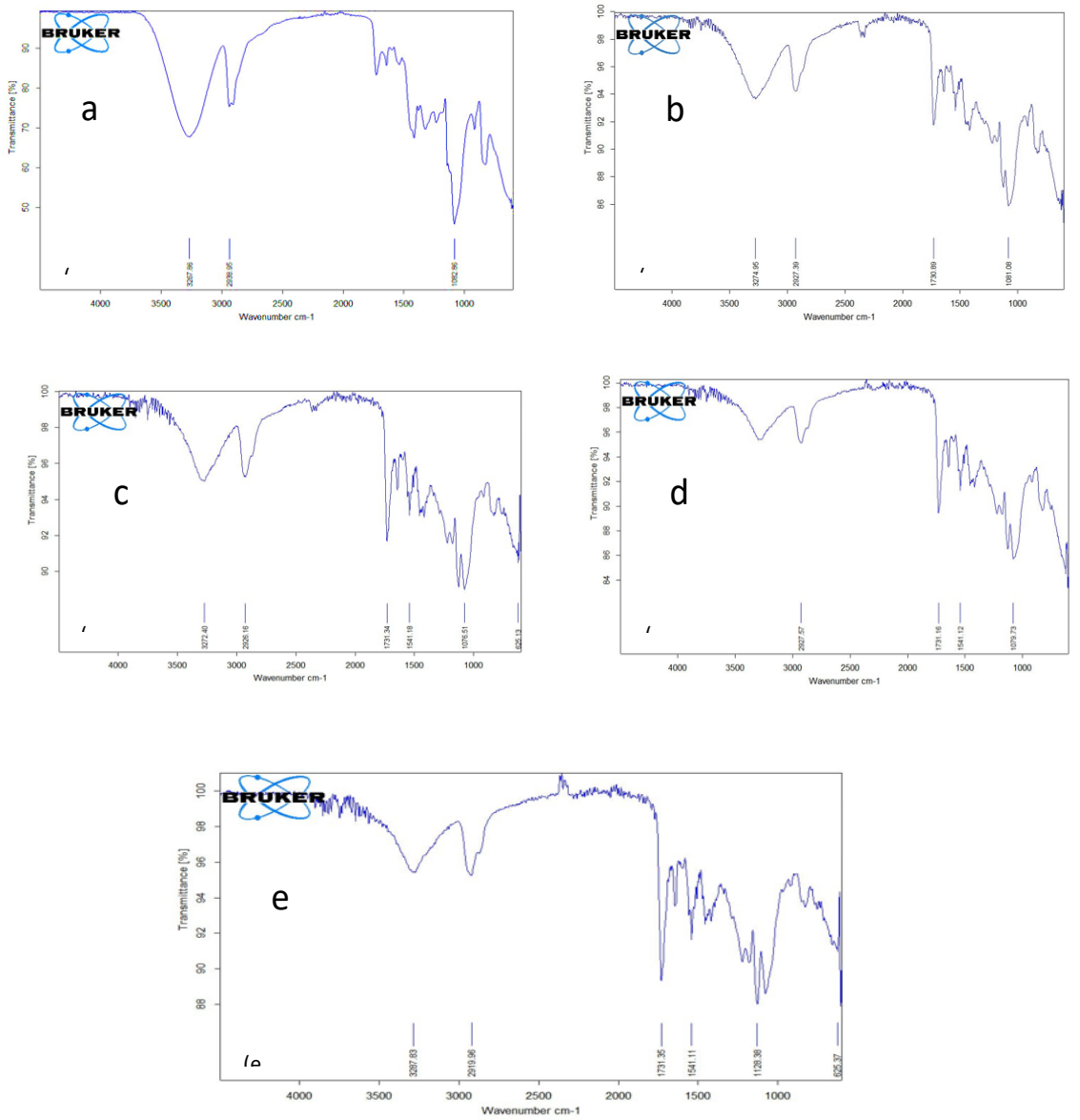


Fig. 3. FTIR spectrum for the (a) pure PVA, (b) 1 wt.% $Y_2O_3$ and $SrCO_3$ NPs, (c) 2 wt.% $Y_2O_3$ and $SrCO_3$ NPs, (d) 3 wt.% $Y_2O_3$ and $SrCO_3$ NPs, (e) 4wt.% $Y_2O_3$ and $SrCO_3$ NPs

grain size decreased with increasing concentration of $Y_2O_3$ and $SrCO_3$ NPs, which decreased from 133 nm for 1% wt. of $Y_2O_3$and $SrCO_3$ NPs to 74 nm for 4% wt. of $Y_2O_3$ and $SrCO_3$ NPs concentration, which indicate a good homogenous distribution. This result is agreed with researches [18].

The newly synthesized pure PVA and PVA/ $Y_2O_3$/ $SrCO_3$ nanocomposite were characterized using FTIR spectroscopy. The FTIR spectra of pure PVA and PVA with different concentrations of $Y_2O_3$ and $SrCO_3$ nanoparticles, ranging from (500 to 4000) $cm^{-1}$, are shown in Fig. 3. In image (a), the pure PVA exhibits a wide absorption band at 3272.40 $cm^{-1}$, which is attributed to the stretching vibration of the alcohol group (OH) in the polymer matrix chain [19]. The C-H group exhibits symmetric stretching vibrations with a frequency of 2926.16 $cm^{-1}$. The vibrational band observed at a wavenumber of 1731.34 $cm^{-1}$ was assigned to the stretching vibration of the C=C bond, whereas the bending vibration of the O–H bond was identified at 1661.22 $cm^{-1}$. The distinctive absorption of chitosan occurs at 1541.18 $cm^{-1}$, corresponding to the stretching vibration of the amino group in chitosan. The C-H group exhibited a bending vibration at a wavenumber of 1441.23 $cm^{-1}$. The degrees of crystallinity were determined using Infrared Spectroscopy by analyzing the peak at 1128.38 $cm^{-1}$ [20, 21]. The magnitude of this peak is affected by the crystalline component of the polymeric chains. Based on the literature [22, 23], this peak corresponds to the symmetric stretching mode of the C-C bond or the stretching of the C-O bond in a specific part of the chain. In this region, an intramolecular hydrogen bond is created between two adjacent OH groups that are on the same side of the carbon chain plane [23]. The C-O stretching vibrations were seen at a wavenumber of 1082.86 $cm^{-1}$. Furthermore, the peaks detected at 845.02 and 625.13 $cm^{-1}$ can be ascribed to the twisting vibration of robust C-O-C and moderate C=C bending vibrations [24].

From the additive concentration (1, 2, 3 and 4) wt. % from $Y_2O_3$ and $SrCO_3$ NPs to PVA polymer in images b, c, d and e caused change in intensities in some band and shift in other band. From this figure, the additive $Y_2O_3$ and $SrCO_3$ NPs caused interaction with polymer matrix. The FTIR proven that there are no interactions between PVA polymer matrix and $Y_2O_3$ and $SrCO_3$ NPs. This result is agreed with researchers [25].

Fig. 4 illustrates the optical absorbance of pure PVA and PVA/ $Y_2O_3$/$SrCO_3$ nanocomposites within the wavelength range of 200-1100 nm. This graphic demonstrates that all samples exhibit much higher absorption in the UV area compared to PVA. When exposed to high energy levels, namely at a wavelength of 200 nm, the electrons in the donor material were prompted to transition into the conduction band. This process occurred

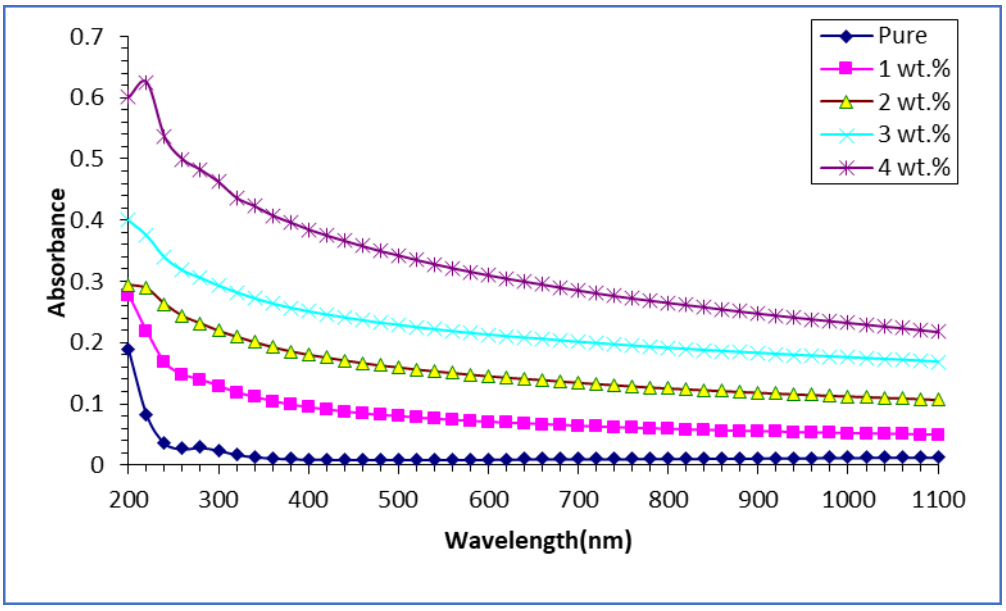


Fig. 4. The absorbance of pure PVA and PVA/ $Y_2O_3$/$SrCO_3$ NPs nanocomposite with wavelength

when the electrons absorbed a photon with a specific energy, causing them to transition from a lower energy state to a higher energy state. In addition, the absorbance is increased by raising the contribution ratio from 0 weight percent of $Y_2O_3$ and $SrCO_3$ nanoparticles to 4 weight percent of $Y_2O_3$ and $SrCO_3$ nanoparticles, respectively. At a wavelength of 200 nm, the absorbance increased from 0.60 to 0.082 with a 41% increase in concentration from 0 to 4 wt.% for $Y_2O_3$ and $SrCO_3$ NPs. However, at wavelengths ranging from 400 to 1100 nm, the absorbance decreased to 0.38 for 4 wt.% $Y_2O_3$ and $SrCO_3$ NPs and 0.0009 for 0 wt.% $Y_2O_3$ and $SrCO_3$ NPs. The conclusion

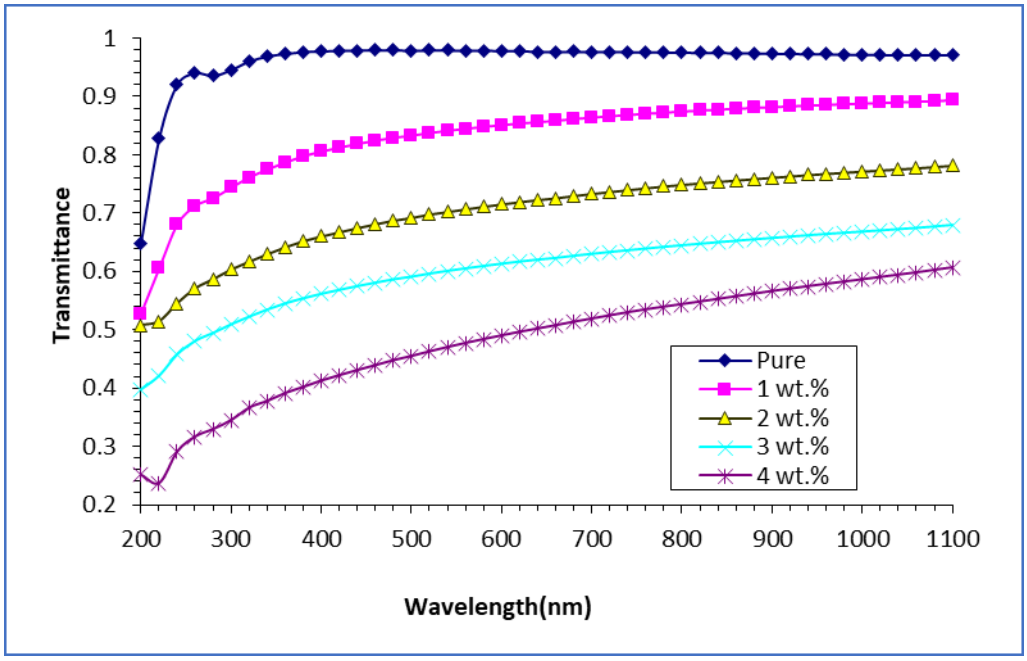


Fig. 5. the transmittance of pure PVA and PVA/ $Y_2O_3$/$SrCO_3$ NPs nanocomposite with wavelength

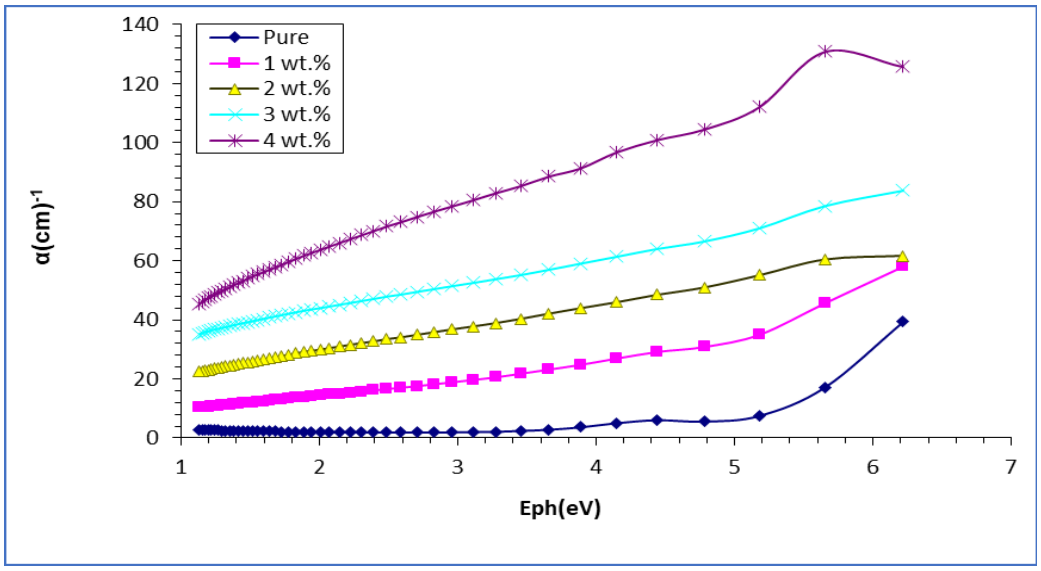


Fig. 6. the absorption coefficient of pure PVA and PVA/ $Y_2O_3$/$SrCO_3$ NPs nanocomposite with wavelength

can be attributed to the inadequate energy of incident photons with longer wavelengths, which hinders their interaction with atoms and enables the photon to pass through. These findings corroborated the information presented in the literature [26, 27]

.The transmittance (T) given by the relation [28]:

$$T = e^{-\alpha t} \quad (1)$$

Where α is the absorption coefficient and t are the thickness of film. Fig. 5 depicts the

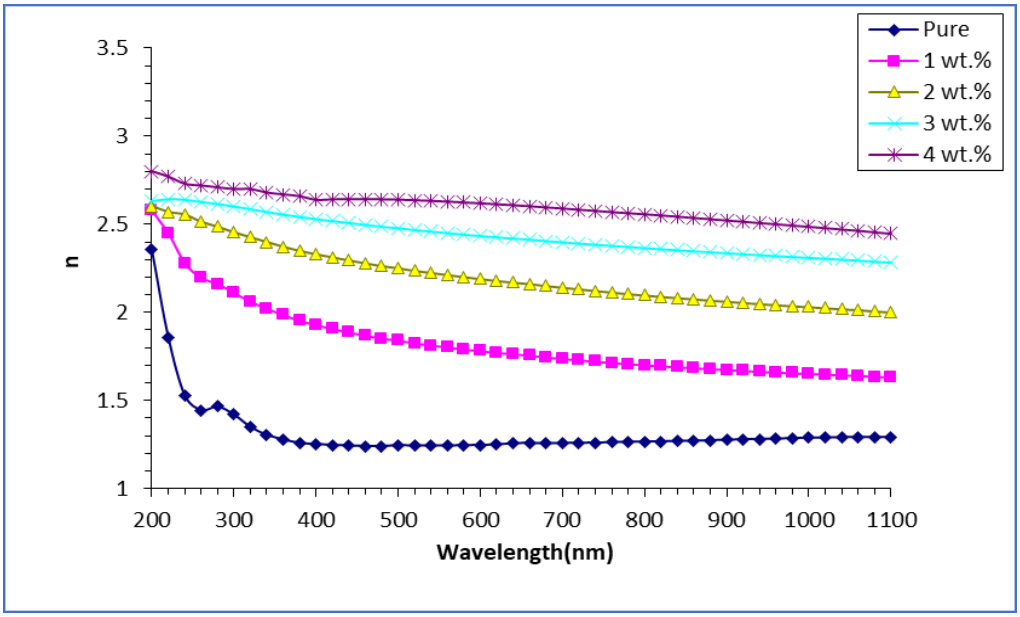


Fig. 7. the refractive index of pure PVA and PVA/ $Y_2O_3$/$SrCO_3$ NPs nanocomposite with wavelength

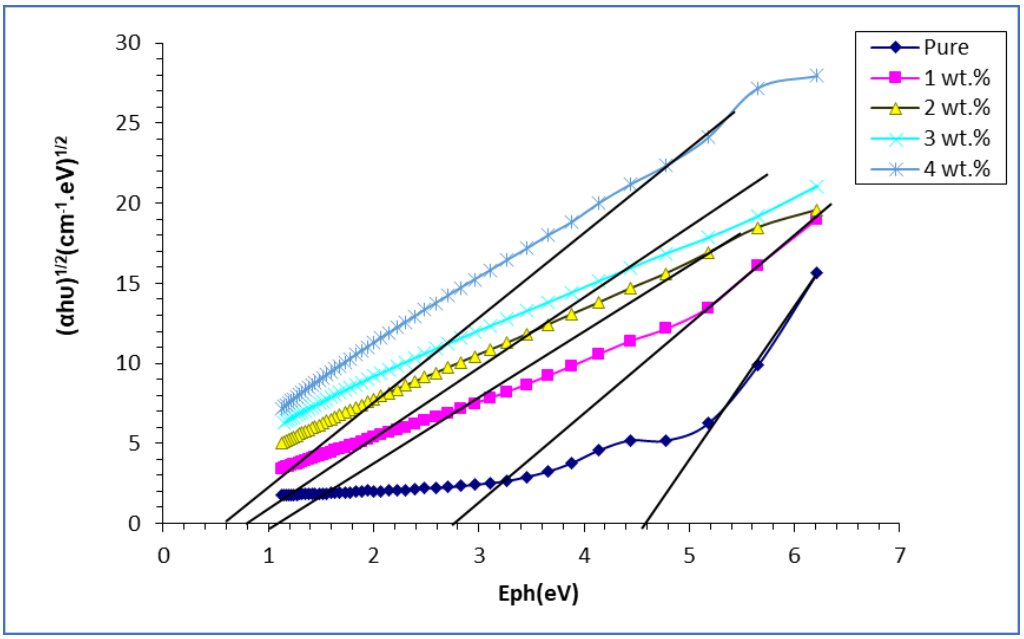


Fig. 8. Relation between $(\alpha h\nu)^{½}$ versus $(h\nu)$ for pure PVA and PVA/ $Y_2O_3$/$SrCO_3$ NPs nanocomposite with wavelength

transmittance (T) spectra of PVA/$Y_2O_3$/$SrCO_3$ nanocomposites at various wavelengths. The figure displays a notable increase in transmittance as the wavelength increases, namely in the vicinity of 220 nm. After reaching this point, the transmittance experiences a relatively stable and consistent increase. The data clearly indicated that the presence of $Y_2O_3$ and $SrCO_3$ NPs resulted in a reduction in light transmittance. The observed behavior was improved by increasing the proportion of $Y_2O_3$ and $SrCO_3$ in the polymer PVA matrix, which explains that the enhancement of nanomaterials led to a rise in light absorption and a decline in transmittance. This result is agreed with researchers [29].

The absorption coefficient (α) of the polymer PVA and its nanocomposite films is employed as a diagnostic tool to quantify the decrease in light intensity within the film. Alternatively, α is a highly responsive physical method that yields excellent insights about the nature of charges within a band and the magnitude of the band gap energy. The accuracy of this data is depending upon the energy level of the incident light. An empirical correlation was utilized to get the absorption coefficient [29].

$$\alpha = 2.303\frac{A}{t} \quad (2)$$

Where A is the absorbance. The Fig. 6 illustrates the relationship between the absorption coefficient (α) of PVA/$Y_2O_3$/$SrCO_3$ nanocomposite films and photon energy. The absorption coefficient exhibited a steady rise in values with increasing photon energy, eventually reaching a value of 4.14 eV. This can be attributed to the electron's lower transition, wherein the energy of the incident photon was not enough to move the electron from the valence band to the conduction

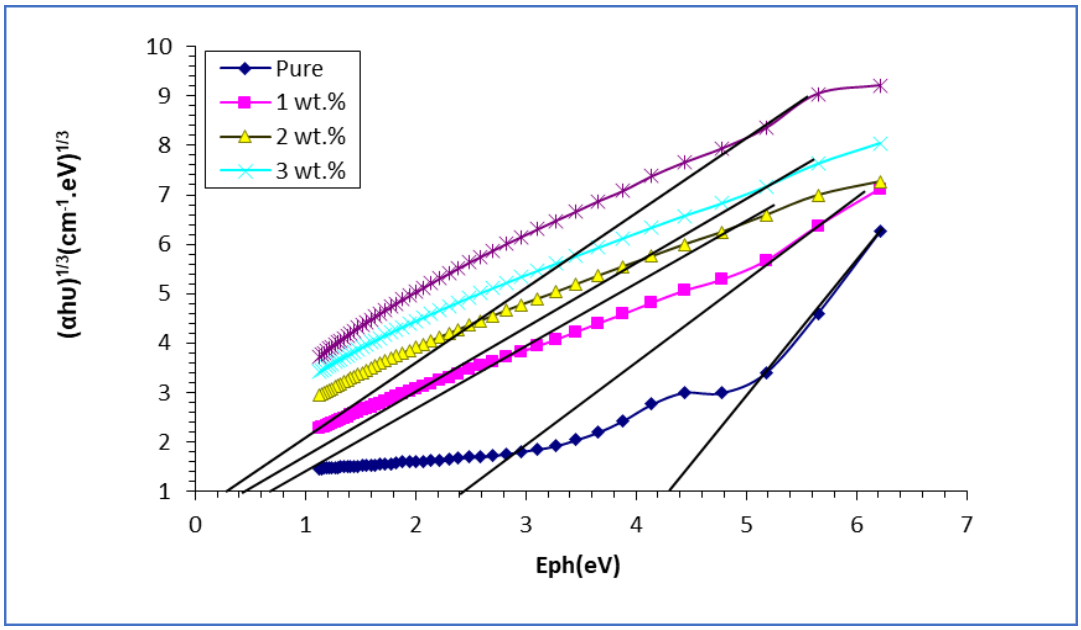


Fig. 9. Relation between $(\alpha h\nu)^{1/3}$ versus $(h\nu)$ of pure PVA and PVA/ $Y_2O_3$/$SrCO_3$ NPs nanocomposite with wavelength

Table 1 Summarized the purification of pure PVA and nanocomposite films.

| wt.% $Y_2O_3$ and $SrCO_3$ NPs | Allowed Eg (eV) | Forbidden Eg (eV) |
|---|---|---|
| 0 | 4.6 | 4.31 |
| 1 | 2.8 | 2.4 |
| 2 | 1 | 0.78 |
| 3 | 0.8 | 0.4 |
| 4 | 0.6 | 0.36 |

band. Upon attaining an energy level of 4.14 eV, the absorption coefficient of all samples demonstrates a notable augmentation. This phenomenon can be attributed to the electron undergoing significant

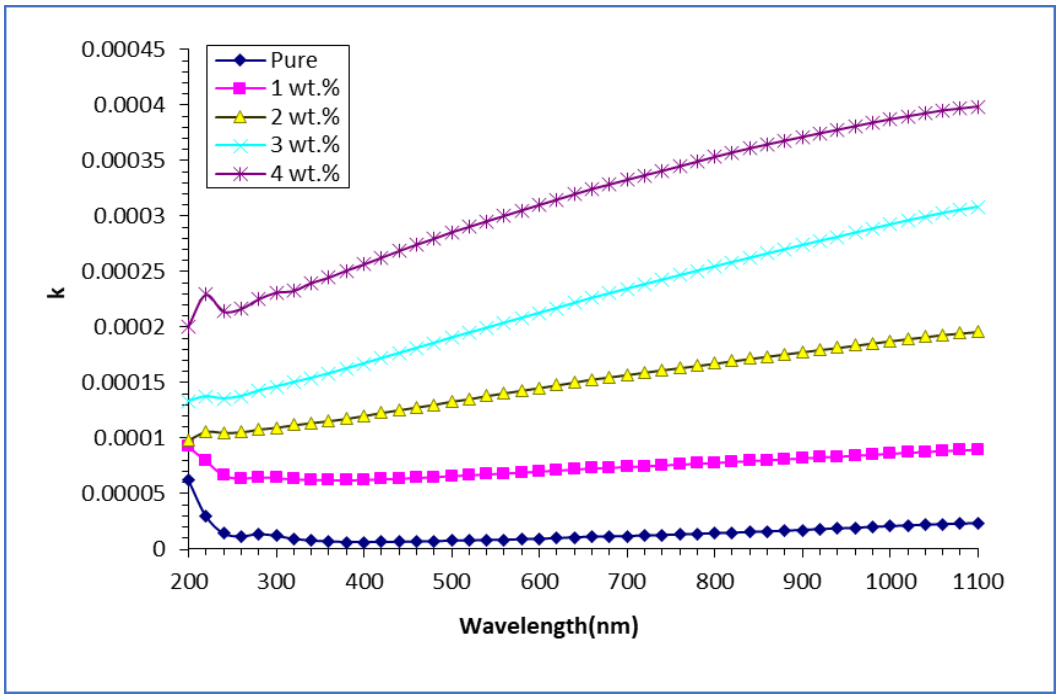


Fig. 10. Extinction coefficient of pure PVA and PVA/ $Y_2O_3$/$SrCO_3$ NPs nanocomposite with wavelength

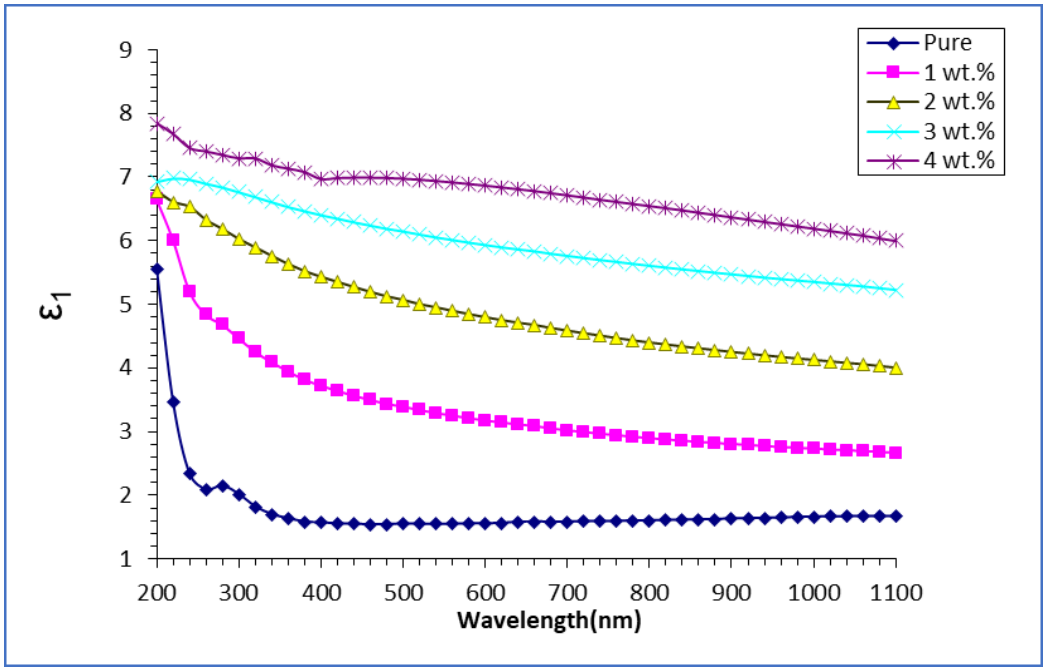


Fig. 11. Real dielectric constant of pure PVA and PVA/ $Y_2O_3$/$SrCO_3$ NPs nanocomposite with wavelength

transitions inside the conductive band. The absorption value is less than $10^4$ $cm^{-1}$, therefore the happened indirect transition.

The index of refractive (n) was calculated from relation [29].

$$n = \frac{1+\sqrt{R}}{1-\sqrt{R}} \quad (3)$$

where R is the reflectance. Fig. 7 depicts the refractive index curves of PVA/$Y_2O_3$/$SrCO_3$ nanocomposites versus with wavelength. Incorporating $Y_2O_3$ and $SrCO_3$ NPs into the polymer matrix resulted in an increase in the refractive index of the samples. This interaction results in the electrons becoming linked to the oscillating electromagnetic field, and as the amount of $Y_2O_3$ and $SrCO_3$ NPs rises, the refractive index values likewise increase. This behavior is agreement with the previous studies [30].

The energy gap is given by [31]:

$$(\alpha h\upsilon)^{1/m} = C(h\upsilon - Eg) \quad (4)$$

For any constant C, the photon energy is denoted as hυ, the energy gap is represented as Eg, and m can take on the values of 2 and 3 for allowed and forbidden indirect transitions, respectively.

The determination of the band gap energy (Eg) involves plotting a graph that relates the product of the absorption coefficient (αhν) and the photon energy (hν). The value of (r) in this equation can be either (1/2) or (1/3), depending on whether the electron transition is allowed or forbidden indirect. The optical band gap values are determined by extrapolating the linear segments of these relationships to the hν axis and are documented in Table 2. Figs. 8 and 9 illustrate the indirect band gap of both pure PVA and PVA/ $Y_2O_3$/$SrCO_3$ nanocomposite. From this figure, it is observed that the $E_g$ decreased with rising of concentration of $Y_2O_3$ and $SrCO_3$ NPs. The allowed indirect energy gap has lowered from 4.6 to 0.6 eV, while the forbidden indirect energy gap has decreased from 4.31 to 0.36 eV. This outcome is related to the possibility of localized states of different color centers extending into the mobility gap. This result agreement with the previous studies [32, 33].

The extinction coefficient ($K_o$)is given by the relation [34]

$$k = \alpha\lambda/4\pi \quad (5)$$

where λ is the wavelength. Fig. 10 displays the

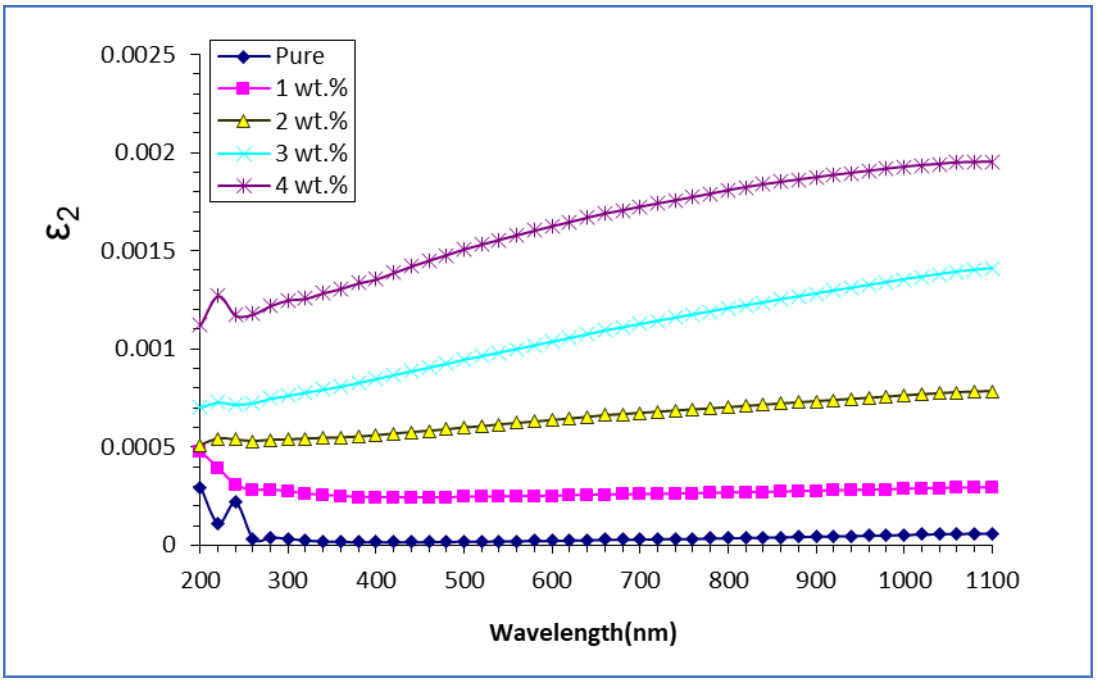


Fig. 12. Imaginary dielectric constant of pure PVA and PVA/ $Y_2O_3$/$SrCO_3$ NPs nanocomposite with wavelength

relationship between the attenuation coefficient and the wavelength for all the films that were made. The extinction coefficient for PVA/$Y_2O_3$/$SrCO_3$ nanocomposites has a distinct peak at lower energies, precisely at a wavelength of 240 nm, followed by a decline at a wavelength of 260 nm. Above 260 nm, the extinction coefficient exhibited a linear increase as the $Y_2O_3$ and $SrCO_3$ nanoparticles increased. This behavior can be ascribed to the simultaneous increase in photon energy. The relationship between the concentration ratio of $Y_2O_3$ and $SrCO_3$ nanoparticles

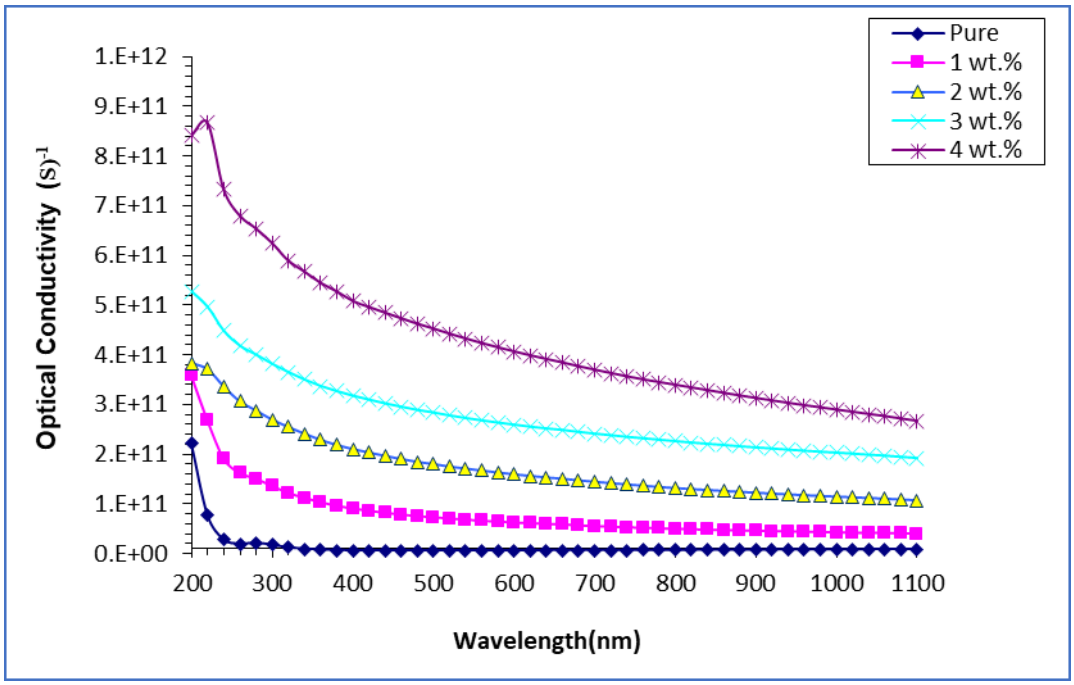


Fig. 13. Optical conductivity of pure PVA and PVA/ $Y_2O_3$/$SrCO_3$ NPs nanocomposite with wavelength

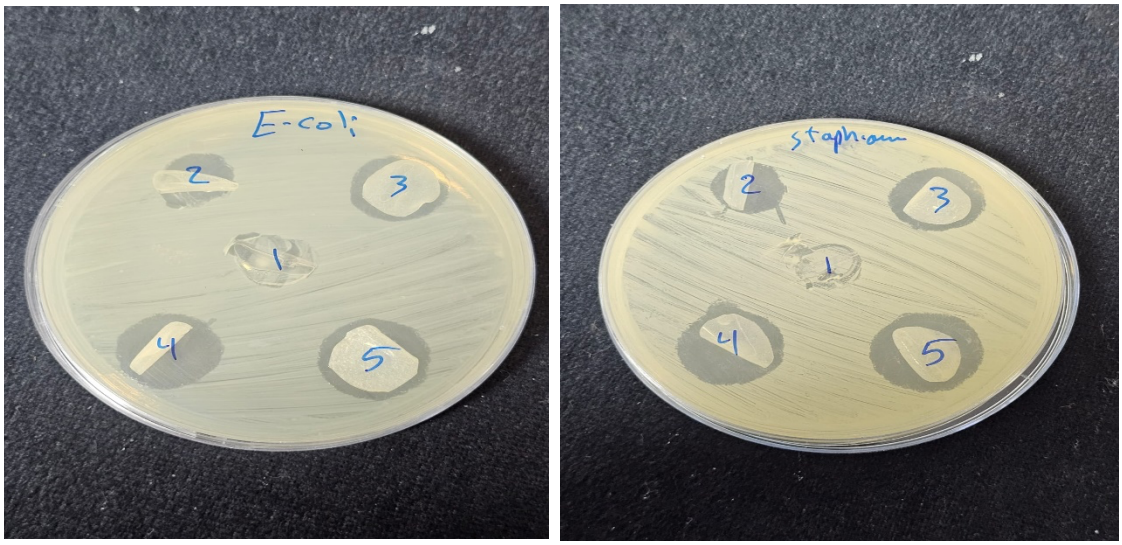


Fig. 14. Image for inhibition zones of PVA/$Y_2O_3$/$SrCO_3$ nanocomposites with different concentration on S. aureus and E. coli

Table 3. Diameter of inhibition zone (mm) of PVA/$Y_2O_3$/$SrCO_3$ nanocomposites on S. aureus and E. coli

| Concentration of $Y_2O_3$/$SrCO_3$ NPs | E. Coli | S. Aureus |
|---|---|---|
| 0 | 0 | 0 |
| 1 | 0 | 0 |
| 2 | 16 | 15 |
| 3 | 18 | 17 |
| 4 | 20 | 19 |

and the extinction coefficient of nanocomposites is clearly evident. This behavior can be attributed to an augmentation in the assimilation of incident light. [35].

The dielectric constant is composed of two parts: the real part ($\varepsilon_1$) and the imaginary part ($\varepsilon_2$) [36]:

$$\varepsilon_1 = n^2 - k^2 \quad (6)$$

$$\varepsilon_2 = 2nk \quad (7)$$

Figs. 11 and 12 depict the fluctuations found in the real component ($\varepsilon_1$) and imaginary component ($\varepsilon_2$) of the dielectric constant for PVA/$Y_2O_3$/$SrCO_3$ nanocomposites. The data demonstrates that the dielectric constant of pure PVA polymer exhibits higher values for both the real and imaginary components at shorter wavelengths, and decreases as the wavelength increases. The nanocomposite films exhibit a significant rise in both the actual and imaginary values as the wavelength decreases. Subsequently, there is a significant decline in energy levels that are greater in magnitude. The apparent similarity can be explained by the fact that the effective dielectric constant is mostly affected by the magnitudes of (n) rather than (k), given that the latter values are significantly smaller than the refractive index, especially when squared [37].

The optical conductivity ($\sigma_{op}$) is definite by [38]:

$$\sigma_{op} = \alpha nc/4\pi \quad (8)$$

where c is the speed of light. Fig.13 illustrates the optical conductivity of the nanocomposites made from PVA, $Y_2O_3$ and $SrCO_3$. The PVA polymer exhibits a significant increase in optical conductivity at shorter wavelengths, followed by a decrease at longer wavelengths. This behavior can be attributed to the simultaneous rise in the absorption coefficient. The correlation between the concentration of $Y_2O_3$ and $SrCO_3$ nanoparticles and the observed optical conductivity is determined to be directly proportional. The observed occurrences can be attributed to the increase in the absorption coefficient [39-41].

We evaluated the antibacterial activity of PVA/$Y_2O_3$/$SrCO_3$ nanocomposites against gram-positive Staphylococcus aureus (S. aureus) and gram-negative Escherichia coli (E. coli). Fig. 14 display the outcomes of these tests at the different concentrations. As the figure shows, the nanocomposite films' inhibition zone against gram-positive (S. aureus) compounds was greater than its inhibition zone against gram-negative (E. coli) compounds. Table 3 shows how the diameter of the inhibitory zone grows with increasing concentration of $Y_2O_3$ and $SrCO_3$ NPs peaking at 20 mm for the gram-negative bacteria (E. coli). Reactive oxygen species (ROS) produced by nanoparticles are thought to be responsible for the antibacterial qualities of nanostructures. Bacteria have negative charges, whereas nanocomposite nanoparticles contain positive charges. Consequently, the bugs will experience oxidation and immediate death due to the electromagnetic contact. Singlet oxygen ($^1O_2$) most likely causes the breakdown of bacterial proteins and DNA. Reactive oxygen species (ROS), including radicals such as superoxide ($O^{-2}$), hydroxyl (OH), and hydrogen peroxide ($H_2O_2$) [42], mainly cause the antibacterial activities of nanocomposites containing nanoparticles.

## CONCLUSION

This work presents a brief summary of a highly effective casting method used in the production of PVA/ $Y_2O_3$/$SrCO_3$ nanocomposites. The OM pictures demonstrated the emergence of interconnected pathways inside the polymeric matrix as electrically charged particles, which intensified

with greater concentrations of nanoparticles. The Field Emission Scanning Electron Microscopy (FESEM) analysis revealed that the $Y_2O_3$ and $SrCO_3$ nanoparticles were evenly dispersed and uniformly distributed throughout the polymer PVA matrix. FTIR analysis confirmed the presence of a tangible interaction between $Y_2O_3$/$SrCO_3$ and the PVA polymer matrix. An increase in the ratio of $Y_2O_3$/$SrCO_3$ in the PVA led to higher absorbance, absorption coefficient, refractive index, extinction coefficient, real and energy band gap. However, it caused a decrease in transmittance and indirect energy gap. The absorption coefficient is below $10^4$ $cm^{-1}$, indicating the occurrence of an indirect electron transition. Finally, the PVA/$Y_2O_3$/$SrCO_3$ nanocomposites were examined as antibacterial against gram-positive (Staphylococcus aureus) and gram-negative (Escherichia coli) and exhibited that the inhibition zone diameter increments with the rise in $Y_2O_3$ and $SrCO_3$ content. The nanocomposite exhibited activity against antibacterial.

## CONFLICT OF INTEREST

The authors declare that there is no conflict of interests regarding the publication of this manuscript.

## REFERENCES


1. Moriche R, Sánchez M, Jiménez-Suárez A, Prolongo SG, Ureña A. Electrically conductive functionalized-GNP/epoxy based composites: From nanocomposite to multiscale glass fibre composite material. Composites Part B: Engineering. 2016;98:49-55.
2. Doagou-Rad S, Islam A, Merca TD. An application-oriented roadmap to select polymeric nanocomposites for advanced applications: A review. Polymer Composites. 2019;41(4):1153-1189.
3. Mohammed MK, Abbas MH, Hashim A, Rabee BH, Habeeb MA, Hamid N. Enhancement of Optical Parameters for PVA/PEG/$Cr_2O_3$ Nanocomposites for Photonics Fields. Revue des composites et des matériaux avancés. 2022;34(4):205-209.
4. Elhosiny Ali H, Abdel-Aziz M, Mahmoud Ibrahiem A, Sayed MA, Abd-Rabboh HSM, Awwad NS, et al. Microstructure Study and Linear/Nonlinear Optical Performance of Bi-Embedded PVP/PVA Films for Optoelectronic and Optical Cut-Off Applications. Polymers. 2022;14(9):1741.
5. Hayder N, Hashim A, Habeeb MA, Rabee BH, Hadi AG, Mohammed MK. Analysis of Dielectric Properties of PVA/PEG/$In_2O_3$ Nanostructures for Electronics Devices. Revue des composites et des matériaux avancés. 2022;32(5):261-264.
6. Refaat D, Mosa E, Fikry M, Omar M. A novel polyvinyl alcohol/polyethylene glycol (PVA/PEG) polymeric blend doped with graphene oxide for energy storage devices. ERU Research Journal. 2024;0(0):0-0.
7. Habeeb MA, Hamza LA. Structural, Optical and D.C Electrical Properties of (PVA-PVP-$Y_2O_3$) Films and Their Application for Humidity Sensor. Journal of Advanced Physics. 2017;6(1):1-9.
8. Mills SJ, Kartashov PM, Ma C, Rossman GR, Novgorodova MI, Kampf AR, Raudsepp M. Yttriaite-(Y): The natural occurrence of $Y_2O_3$ from the Bol'shaya Pol'ya River, Subpolar Urals, Russia. American Mineralogist. 2011;96(7):1166-1170.
9. Márquez-Herrera A, Ovando-Medina VM, Castillo-Reyes BE, Meléndez-Lira M, Zapata-Torres M, Saldaña N. A novel synthesis of $SrCO_3$–$SrTiO_3$ nanocomposites with high photocatalytic activity. Journal of Nanoparticle Research. 2014;16(12).
10. Alavi MA, Morsali A. Syntheses and characterization of $Sr(OH)_2$ and $SrCO_3$ nanostructures by ultrasonic method. Ultrason Sonochem. 2010;17(1):132-138.
11. Küther J, Nelles G, Seshadri R, Schaub M, Butt H-J, Tremel W. Templated Crystallisation of Calcium and Strontium Carbonates on Centred Rectangular Self-Assembled Monolayer Substrates. Chemistry - A European Journal. 1998;4(9):1834-1842.
12. Küther J, Bartz M, Seshadri R, Vaughan GBM, Tremel W. Crystallization of $SrCO_3$ on a self-assembled monolayer substrate: an in-situ synchrotron X-ray study. Journal of Materials Chemistry. 2001;11(2):503-506.
13. Sastry M, Kumar A, Damle C, Sainkar SR, Bhagwat M, Ramaswamy V. Crystallization of $SrCO_3$ within thermally evaporated fatty acid films: unusual morphology of crystal aggregates. CrystEngComm. 2001;3(21):81.
14. Cai Q, Ma H. Recent Advances of Chiral Hypervalent Iodine Reagents. Acta Chim Sinica. 2019;77(3):213.
15. Yu J, Guo H, Cheng B. Shape evolution of $SrCO_3$ particles in the presence of poly-(styrene-alt-maleic acid). J Solid State Chem. 2006;179(3):800-803.
16. Rezvanpour M, Hasanzadeh M, Azizi D, Rezvanpour A, Alizadeh M. Synthesis and characterization of micro-nanoencapsulated n -eicosane with PMMA shell as novel phase change materials for thermal energy storage. Materials Chemistry and Physics. 2018;215:299-304.
17. Arasakumari M, Subramanian K. Synthesis and Electrical Properties of Anhydrous GdCl3 Doped PVA Polymer Electrolyte Films. International Journal of Electrochemical Science. 2022;17(7):220720.
18. Rajeswari N, Selvasekarapandian S, Karthikeyan S, Prabu M, Hirankumar G, Nithya H, Sanjeeviraja C. Conductivity and dielectric properties of polyvinyl alcohol–polyvinylpyrrolidone poly blend film using non-aqueous medium. Journal of Non-Crystalline Solids. 2011;357(22-23):3751-3756.
19. Jassim HH, Hashim FS. Synthesis of (PVA/PEG: ZnO and Co3O4) Nanocomposites: Characterization and Gamma Ray Studies. Neuroquantology. 2021;19(4):47-56.
20. Negim E, Rakhmetullayeva R, Yeligbayeva G, Urkimbaeva P, Primzharova S, Kaldybekov D, et al. Improving biodegradability of polyvinyl alcohol/starch blend films for packaging applications. International Journal of Basic and Applied Sciences. 2014;3(3).
21. Olewnik-Kruszkowska E, Gierszewska M, Jakubowska E, Tarach I, Sedlarik V, Pummerova M. Antibacterial Films Based on PVA and PVA-Chitosan Modified with Poly(Hexamethylene Guanidine). Polymers. 2019;11(12):2093.
22. Hydrogels in Medicine and Pharmacy. CRC Press; 2019.
23. Mallapragada SK, Peppas NA, Colombo P. Crystal

dissolution-controlled release systems. II. Metronidazole release from semicrystalline poly(vinyl alcohol) systems. J Biomed Mater Res. 1997;36(1):125-130.
24. Mansur HS, Sadahira CM, Souza AN, Mansur AAP. FTIR spectroscopy characterization of poly (vinyl alcohol) hydrogel with different hydrolysis degree and chemically crosslinked with glutaraldehyde. Materials Science and Engineering: C. 2008;28(4):539-548.
25. El-Kader MFHA, Elabbasy MT, Adeboye AA, Menazea AA. Nanocomposite of PVA/PVP blend incorporated by copper oxide nanoparticles via nanosecond laser ablation for antibacterial activity enhancement. Polym Bull. 2021;79(11):9779-9795.
26. Abdali K, Rabee BH, Al-Bermany E, Abdulridha AR, Abass KH, Kadim AM. Effect of Doping $Sb_2O_3$ NPs on Morphological, Mechanical, and Dielectric Properties of PVA/PVP Blend Film for Electromechanical Applications. Nano. 2023;18(03).
27. Luo Q, Shan Y, Zuo X, Liu J. Anisotropic tough poly(vinyl alcohol)/graphene oxide nanocomposite hydrogels for potential biomedical applications. RSC advances. 2018;8(24):13284-13291.
28. Mohammed MK, Al-Dahash G, Al-Nafiey A. Fabrication and Characterization of the PMMA/G/Ag Nanocomposite by Pulsed Laser Ablation (PLAL). Nano Biomed Eng. 2022;14(1).
29. Khadayeir AA, Hassan ES, Chiad SS, Habubi NF, Abass KH, Rahid MH, et al. Structural and Optical Properties of Boron Doped Cadmium Oxide. Journal of Physics: Conference Series. 2019;1234(1):012014.
30. Salloom HT, Jasim AS, Hamad TK. Synthesis and Optical Characterization of Ag/PVA Nanocomposites Films. Journal of Al-Nahrain University Science. 2017;20(4):56-63.
31. Mousavi SS, Sajad B, Majlesara MH. Fast response ZnO/PVA nanocomposite-based photodiodes modified by graphene quantum dots. Materials & Design. 2019;162:249-255.
32. Zidan HM, Abdelrazek EM, Abdelghany AM, Tarabiah AE. Characterization and some physical studies of PVA/PVP filled with MWCNTs. Journal of Materials Research and Technology. 2019;8(1):904-913.
33. Zidan HM, Abu-Elnader M. Structural and optical properties of pure PMMA and metal chloride-doped PMMA films. Physica B: Condensed Matter. 2005;355(1-4):308-317.
34. Al-Abbas SS, Ghazi RA, Al-shammari AK, Aldulaimi NR, Abdulridha AR, Al-Nesrawy SH, Al-Bermany E. Influence of the polymer molecular weights on the electrical properties of Poly(vinyl alcohol) – Poly(ethylene glycols)/Graphene oxide nanocomposites. Materials Today: Proceedings. 2021;42:2469-2474.
35. Mireles LK, Wu M-R, Saadeh N, Yahia LH, Sacher E. Physicochemical Characterization of Polyvinyl Pyrrolidone: A Tale of Two Polyvinyl Pyrrolidones. ACS omega. 2020;5(47):30461-30467.
36. Soliman TS, Vshivkov SA, Elkalashy SI. Structural, thermal, and linear optical properties of $SiO_2$ nanoparticles dispersed in polyvinyl alcohol nanocomposite films. Polymer Composites. 2020;41(8):3340-3350.
37. Fal J, Bulanda K, Traciak J, Sobczak J, Kuzioła R, Grąz KM, et al. Electrical and Optical Properties of Silicon OxideLignin Polylactide ($SiO_2$-L-PLA). Molecules (Basel, Switzerland). 2020;25(6):1354.
38. Al-Rubaye SAJ, A. Al-lsawi N, Abdulridha AR. Preparation and Study the Electrical and Optical Properties for (PVA-PEG-Sr2O3) Nanocomposites. Neuroquantology. 2021;19(10):47-55.
39. Abid AA, Al-nesrawy SH, Abdulridha AR. New Fabrication (PVA-PVP-C. B) Nanocomposites: Structural and Electrical Properties. Journal of Physics: Conference Series. 2021;1804(1):012037.
40. Jabbar SA, Khalil SM, Abdulridha AR, Al-Bermany E, Karar A. Dielectric, AC Conductivity and Optical Characterizations of (PVA-PEG) Doped SrO Hybrid Nanocomposites. Key Eng Mater. 2022;936:83-92.
41. Al-Kateb DE, Abdulridha AR. Structural and Optical Properties of (PVA/PVP:$Sr_2NO_3$) Nanocomposites. Neuroquantology. 2021;19(4):27-37.
42. Aunkor MTH, Raihan T, Prodhan SH, Metselaar HSC, Malik SUF, Azad AK. Antibacterial activity of graphene oxide nanosheet against multidrug resistant superbugs isolated from infected patients. Royal Society open science. 2020;7(7):200640-200640.